A Novel Approach for Kinematic Analysis and Workspace Optimization of a Redundant Full Rotation Planar Parallel Manipulator

Henrique Simas, Luan Meneghini, and Roberto Simoni

Abstract Planar Parallel Mechanisms (PPMs) with full rotational capability (FRPPMs) are essential for applications that demand precise, high-speed motion and continuous 360-degree orientation control, overcoming the workspace limitations and singularities inherent to conventional 3-DOF architectures. Kinematic redundancy is commonly applied in robotic systems to achieve full rotation; however, it generally leads to hybrid structures that compromise the original manipulator's load transfer properties. This paper focuses on an existing redundantly actuated FRPPM that preserves the structural advantages of a purely parallel architecture while providing geometric adaptability and reconfigurability. The study investigates and extends the instantaneous kinematic model by explicitly incorporating the platform's passive rotation angle into the formulation. Additionally, a workspace optimization strategy based on the transmission angle is proposed to enhance motion and force transmission while avoiding near-singular configurations. This approach improves the operational efficiency and adaptability of the mechanism in confined or irregular environments, providing a consistent and robust framework for high-performance planar motion with unlimited orientation capability.

H. Simas
Federal University of Santa Catarina, Florianopolis, Santa Catarina, Brazil
e-mail: henrique.simas@ufsc.br

L. Meneghini
Federal University of Santa Catarina, Florianopolis, Santa Catarina, Brazil

R. Simoni
Federal University of Santa Catarina, Florianopolis, Santa Catarina, Brazil

1 Introduction

A FRPPM is a type of PPM that provides continuous 360-degree rotation (full rotation) around an axis in the plane [1]. These FRPPM are often used in applications that require precise, high-speed planar motion with full orientation control. Traditional 3-DOF architectures, such as the 3-RPR and 3-PRR, are often limited to less than 180° due to singularities [1]. To overcome this drawnback, Gosselin et al. [1] introduced kinematically redundant PPM with 4-DOF, enabling full-cycle rotation by avoiding these singular configurations.

While kinematic redundancy is widely recommended to mitigate singularities [2, 3] by adding actuators or joints, some strategies result in hybrid designs that compromise the parallel structure's load transfer properties. In contrast, Variable-Configuration Parallel Manipulators with Self-Aligning (VCPMSA) offer structural adaptability in the base, legs, or platform [4] without affecting the end-effector's motion characteristics. Utilizing passive or null DOF, VCPMSA like the TRIFLEX I and II [4, 5], the KCL/TJU metamorphic hand [6], Tetraflex [7], feature reconfigurable bases and self-aligning joints. These attributes provide adjustable workspaces, geometric adaptability for confined environments, and enhanced portability.

This paper focuses on the FRPPM proposed by [1] which can change the base geometry and become a VCPMSA. This work extends the original instantaneous kinematics model by incorporating the platform's passive angle and applying workspace optimization based on the transmission quality.

2 A geometric approach to the generalized full rotational planar mechanism

Figure 1 illustrates the generalized VCPMSA, part of a family proposed by Gosselin et al. [1]. This 4-PRR configuration comprises four identical legs organized into two kinematic loops ($i = 1, 2$), where each loop is defined by the connection of two legs corresponding to a branch index $j = 1, 2$. The four legs are identified using double subscript notation ij (11, 12, 21, and 22), with i denoting the loop and j the leg within that loop. Each leg ij comprises a link of length a_{ij} and an actuated prismatic joint with displacement d_{ij}, which, by being fixed to the ground, allows the manipulator to achieve variable configuration properties.

The end-effector consists of link e_1 (as shown in Fig. 1), with its position defined by the coordinates of point E and its orientation described by angles α. Redundancy is introduced through the additional actuated leg 22, which provides the control input angle φ and, as noted by Gosselin et al. [1], enables the end-effector to perform unlimited rotation about point E.

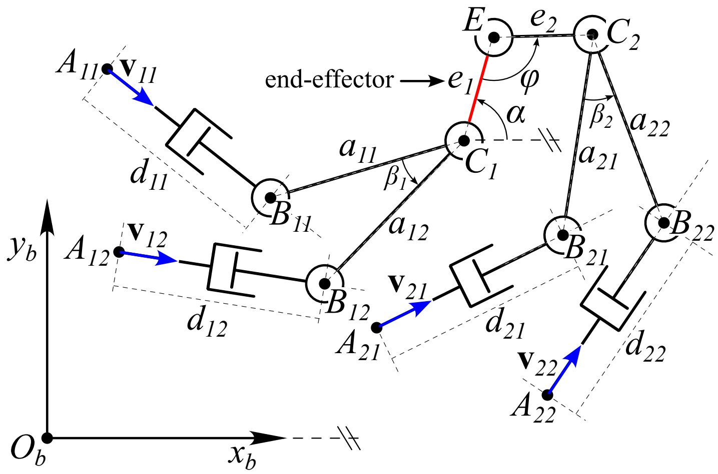

Fig. 1: Generalized full rotation VCPMSA. Adapted from Gosselin et al. [1].

2.1 Geometric Modelling

Inspecting Fig. Mathematical formulation for each leg provides:

$$B_{ij} = A_{ij} + d_{ij}\,\mathbf{v}_{ij} \tag{1}$$

$$(C_i - B_{ij}) \cdot (C_i - B_{ij}) = a_{ij}^2 \tag{2}$$

Substituting Eq. (1) into Eq. (2) and solving the dot product yields:

$$d_{ij}^2 + 2d_{ij}(\mathbf{v}_{ij} \cdot \mathbf{w}_{ij}) + \mathbf{w}_{ij} \cdot \mathbf{w}_{ij} - a_{ij}^2 = 0 \tag{3}$$

where $\mathbf{w}_{ij} = A_{ij} - C_i$.

By inspecting the VCPMSA, the relationship between the serial chain connecting C_1 and C_2, the position of the revolute joint E, and each of the kinematic closed loops can be established as follows. For kinematic loop $i = 1$ and kinematic loop $i = 2$, respectively,

$$E = C_1 + e_1[c_\alpha \;\, s_\alpha]^T \qquad E = C_2 + e_2[c_{\alpha\varphi} \;\, s_{\alpha\varphi}]^T \tag{4}$$

where s_* and c_* are $\sin(*)$ and $\cos(*)$, respectively.

Equations (3) and (4) provide the closure loop with input variables given by the prismatic joint displacements composing the tuple $\mathbf{d} = [d_{11} \;\, d_{12} \;\, d_{21} \;\, d_{22}]^T$ while the Cartesian variables are the coordinates in the $x_b y_b$-plane augmented by the angles α and φ, composing the output tuple$\mathbf{x} = \left[E_x \;\, E_y \;\, \alpha \;\, \varphi\right]^T$.

2.2 Position Analysis

Inverse Position Analysis (IPA): The IPA of a VCPMSA is the determination of the actuated joint variables values, i.e., $\mathbf{d} = \left[d_{11}\ d_{12}\ d_{21}\ d_{22}\right]^T$ compatible with one assigned platform pose $\mathbf{x} = \left[E_x\ E_y\ \alpha\ \varphi\right]^T$. Solving the closure Eq. (3), the IPA solution is given by

$$d_{ij} = \left(-d_a \pm \sqrt{d_a^2 - 4d_a d_b}\right)/2d_a \tag{5}$$

where $d_a = 2\big(\mathbf{v}_{ij} \cdot (A_{ij} - C_i)\big)$, and $d_b = (A_{ij} - C_i) \cdot (A_{ij} - C_i) - a_{ij}^2$.

Forward Position Analysis (FPA): The Forward Position Analysis (FPA) of the VCPMSA determines the pose $\mathbf{x} = [E_x\ E_y\ \alpha\ \varphi]^T$ from the actuated-joint variables $\mathbf{d} = [d_{11}\ \ d_{12}\ \ d_{21}\ \ d_{22}]^T$. After computing B_{ij} via Eq. (1), coordinates of C_i are found by intersecting circles centered at B_{ij} with radii a_{ij}. In the auxiliary $\mathbf{v}_\beta\mathbf{v}_{\beta_\perp}$-frame defined by $\mathbf{R}_i = [\mathbf{v}_\beta\ \mathbf{v}_{\beta_\perp}]$, where $\mathbf{v}_\beta = (B_{i2} - B_{i1})/\|B_{i2} - B_{i1}\|$, the local coordinates are calculated as follows,

$$C_{i\beta} = \frac{1}{2\|B_{i2} - B_{i1}\|}\begin{bmatrix} a_{i1}^2 - a_{i2}^2 + \|B_{i2} - B_{i1}\|^2 \\ \pm\sqrt{4a_{i1}^2\|B_{i2} - B_{i1}\|^2 - (a_{i1}^2 - a_{i2}^2 + \|B_{i2} - B_{i1}\|^2)^2} \end{bmatrix} \tag{6}$$

The global coordinates $C_i = \mathbf{R}_i C_{i\beta}$ allow for the calculation of point E following the same logic using links e_1, e_2 and rotation matrix $\mathbf{R}_v = [\mathbf{v}_\gamma\ \mathbf{v}_{\gamma_\perp}]$ for $\mathbf{v}_\gamma = (C_2 - C_1)/\|C_2 - C_1\|$. The resulting $E = \mathbf{R}_v E_\gamma$ defines the platform pose, while the orientation is given by $\alpha = \operatorname{atan2}(E_y - C_{1y}, E_x - C_{1x})$. Finally, the angle φ is found via $\varphi = \operatorname{signal}(E_{\gamma y})\cos^{-1}(((C_2 - E)\cdot(C_1 - E))/(e_1 e_2))$, using the chosen signal for $E_{\gamma y}$ from the local frame derivation.

3 Instantaneous kinematics

The FIKP (*Forward instantaneous kinematics position*) involves computing the platform twist (or the time derivatives of pose-defining variables) given the actuated joint rates. Conversely, the IIKP *Inverse instantaneous kinematics position*) consists of determining the required actuated joint rates for a known platform twist or known time derivatives of the platform pose variables.

For the VCPMSA, time derivative of Eq. (3) yields

$$\dot{d}_{ij}\big(d_{ij} + \mathbf{v}_{ij} \cdot (A_{ij} - C_i)\big) + \dot{C}_i \cdot (-d_{ij}\mathbf{v}_{ij} - (A_{ij} - C_i)) = 0. \tag{7}$$

Isolating $\dot{C}_i$ in Eq. (4), followed by taking the time derivative of each expression, yields $\dot{C}_1 = \dot{E} - e_1\mathbf{v}_\alpha\dot{\alpha}$ and $\dot{C}_2 = \dot{E} - e_2\mathbf{v}_{\alpha\varphi}(\dot{\alpha} + \dot{\varphi})$ where $\mathbf{v}_\alpha = [\sin\alpha \quad \cos\alpha]^T$ and $\mathbf{v}_{\alpha\varphi} = [\sin(\alpha + \varphi) \quad \cos(\alpha + \varphi)]^T$. Substituting these results into Eq.(7) yields four differential relationships, which can be compactly expressed in matrix form as follows:

$$\begin{bmatrix} k_{11} & 0 & 0 & 0 \\ 0 & k_{12} & 0 & 0 \\ 0 & 0 & k_{21} & 0 \\ 0 & 0 & 0 & k_{22} \end{bmatrix} \begin{bmatrix} \dot{d}_{11} \\ \dot{d}_{12} \\ \dot{d}_{21} \\ \dot{d}_{22} \end{bmatrix} = \begin{bmatrix} \mathbf{r}_{11} & f_{11} & 0 \\ \mathbf{r}_{12} & f_{12} & 0 \\ \mathbf{r}_{21} & g_{21} & g_{21} \\ \mathbf{r}_{22} & g_{22} & g_{22} \end{bmatrix} \begin{bmatrix} \dot{E}_x \\ \dot{E}_y \\ \dot{\varphi} \\ \dot{\alpha} \end{bmatrix} \Rightarrow \mathbf{M}_d \dot{\mathbf{d}} = \mathbf{M}_x \dot{\mathbf{x}}. \quad (8)$$

where $k_{ij} = d_{ij} + \mathbf{v}_{ij} \cdot (A_{ij} - C_i)$, $f_{ij} = -e_i \, \mathbf{v}_\alpha \cdot (d_{ij}\mathbf{v}_{ij} + (A_{ij} - C_i))$ and $g_{ij} = -e_i \, \mathbf{v}_{\alpha\varphi} \cdot (d_{ij}\mathbf{v}_{ij} + (A_{ij} - C_i))$ are scalar values and $\mathbf{r}_{ij} = [d_{ij}\mathbf{v}_{ij} + (A_{ij} - C_i)]$ a row vector.

3.1 Singularities Analysis

Singularities in parallel manipulators represent configurations where the mapping between platform twist and joint rates breaks down, categorized into Type-I (unsolvable IIKP kinematics), Type-II (unsolvable FIKP kinematics), and Type-III (both). For the VCPMSA, Type-I singularities occur when the kinematic matrix $\mathbf{M}_d$ becomes rank-deficient, defined by the condition $\det(\mathbf{M}_d) = \prod_{i=1}^{2} \prod_{j=1}^{2} (d_{ij} + \mathbf{v}_{ij} \cdot (A_{ij} - C_i)) = 0$. Geometrically, this happens when the projection of $(C_i - A_{ij})$ along the unit vector $\mathbf{v}_{ij}$ equals d_{ij}, meaning the segment $(C_i - B_{ij})$ is perpendicular to $\mathbf{v}_{ij}$.

Type-II singularities arise when $\det(\mathbf{M}_x) = S_1 S_2 S_\varphi = 0$. Here, $S_i = \|B_{i1} \times C_i + C_i \times B_{i2} + B_{i2} \times B_{i1}\|$ represents the area of the triangle formed by B_{i1}, C_i, and B_{i2}, while $S_\varphi = e_1 e_2 \sin(\varphi)/2$ is the area of the triangle formed by C_1, E, and C_2. Geometrically, this occurs when links a_{i1} and a_{i2} become collinear or when links e_1 and e_2 align at $\varphi = k\pi$ rad. Type-III singularities occur when both $S_i = 0$ and the segment $(C_i - B_{ij})$ is perpendicular to $\mathbf{v}_{ij}$.

4 Performance Index

The transmission quality (or transmission angle) is a key performance parameter linked to smooth motion transmission, singularity avoidance, and mechanical advantage [8]. While adequate angles (typically 40° to 140°) ensure efficient force transmission at low speeds, high-speed performance also requires considering dynamic balancing and stiffness [**?**].

Furthermore, transmission angles indicate sensitivity to mechanical errors and the proximity of singularities [9]. For the VCPMSA (Fig. 1), three transmission angles are analyzed: β_i (triangles $B_{i1}C_iB_{i2}$) and φ (triangle C_1EC_2).

Singularities are avoided by maximizing the triangle area $H_i = (l^2 \sin \beta_i)/2$, which occurs at $\beta_i = \pi/2 + n\pi$. Consequently, this study adopts an optimal

90° transmission angle, constrained between 40° and 140° for simulations. Similarly, S_φ is maximized at $\varphi = \pi/2+n\pi$, consistent with [1]; thus, $\varphi = \pi/2$ rad is used for subsequent analyses.

4.1 Workspace optimization analysis

The workspace analysis of the VCPMSA assumes that are known parameters such as base points A_{ij}, link lengths a_{ij} and e_i, and the prismatic joint directions defined by the unit vector $\mathbf{v}_{ij} = [\cos(\theta_{ij})\ \sin(\theta_{ij})]^T$ with displacement limits h_{ij}. Each leg ij generates a sub-workspace SW_{ij} designed to allow full rotation around point E, bounded by two lines parallel to $\mathbf{v}_{ij}$ at distances of $\pm(a_{ij} - e_i)$ and two circular segments centered at A_{ij} and D_{ij} with radii $a_{ij} + e_i$ and $a_{ij} - e_i$.

The final boundaries of each SW_{ij} are determined by the intersection points of these geometric limits, as illustrated in Fig. 2a. To determine the overall workspace W of the VCPMSA, the geometric intersection of all four individual leg sub-workspaces is calculated, resulting in the shared area where W equals the intersection of SW_{11}, SW_{12}, SW_{21}, and SW_{22}. This approach ensures that the manipulator's reachable configurations satisfy the constraints of all four legs simultaneously.

4.2 Useful Workspace and the performance analysis

For the VCPMSA, the objective is to maximize the intersection of leg sub-workspaces SW_{ij}. While individual SW_{ij} are elongated along the axis $\mathbf{v}_{ij}$, their intersection produces a truncated, limited workspace of reduced practical utility. This study proposes the inscription of a square SQ_{ij} within each SW_{ij} . This methodology yields a square or near-square global workspace W, optimizing both the effective prismatic displacement and the resulting intersection region.

Defining the useful sub-workspace SQ_{ij} as a square, and given the link lengths a_{ij} and e_i, the coordinates of A_{ij} and the vector $\mathbf{v}_{ij}$, the coordinates of D_{ij} are obtained as $D_{ij} = A_{ij} + h_{ij}\mathbf{v}_{ij}$, with $h_{ij} = 3a_{ij} - e_i$ representing the effective prismatic displacement, yielding a square sub-workspace SQ_{ij} with side length $L = 2(a_{ij} - e_i)$, as shown in Fig. 2b.

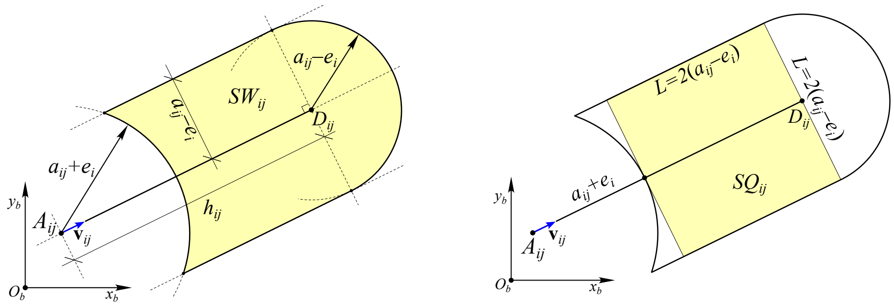

(a) (b)

Fig. 2: (a) Sub-workspace SW_{ij} to the leg ij. (b) Square sub-workspace SQ_{ij}.

5 Dimensional analysis

Maximum intersection of the square sub-workspaces SQ_{ij} occurs when they coincide, requiring vectors $\mathbf{v}_{ij}$ to be parallel or perpendicular. Setting $e_i = 1$ l.u. (where l.u. stands for '*length units*') yields $a_{ij} = (L/2+1)$, and the analysis identifies six distinct orientation combinations $K_n(\theta_{11}, \theta_{12}, \theta_{21}, \theta_{22})$, $n \in \{a, b, c, d, e, f\}$. Without loss of generality, these configurations are defined by $\theta_{ij} \in \{0, \pi/2, \pi, 3\pi/2\}$ rad, specifically: $K_a(0, \pi/2, 0, 3\pi/2)$, $K_b(0, \pi/2, \pi, 3\pi/2)$, $K_c(0, \pi, \pi/2, 3\pi/2)$, $K_d(0, \pi/2, 0, \pi/2)$, $K_e(0, \pi/2, 0, \pi)$, and $K_f(0, \pi, 0, \pi)$, as shown in the Fig. 3.

To determine the optimal configuration, each combination is evaluated based on the maximum and minimum transmission angles [7, 10] throughout the full rotation of the end-effector. For a given square side length $L = 8$ l.u. yields $a_{ij} = 5$ l.u.. For the sub-workspace SQ_{ij} centered at the Cartesian origin, the coordinates are defined as $A_{ij} = -2a_{ij}\mathbf{v}_{ij} = -10\mathbf{v}_{ij}$ and $D_{ij} = (a_{ij} - e_i)\mathbf{v}_{ij} = 4\mathbf{v}_{ij}$. This configuration provides an effective prismatic displacement range of $h_{ij} = 14$ l.u.

5.1 Discussion

Figure 4 shows the dimensional analysis demonstrating, that the orientation of the prismatic joint axes, defined by the unit vectors $\mathbf{v}_{ij}$, governs the topological characteristics of the resultant workspace. While the six identified combinations (K_a through K_f) utilize identical geometric constraints, variations in $\mathbf{v}_{ij}$ influence sub-workspace overlap and the transmission quality. Consequently, the selection of $\mathbf{v}_{ij}$ minimizes sensitivity to mechanical errors and maximizes the distance from singular configurations by maintaining the transmission angle within the $90° \pm 50°$ interval.

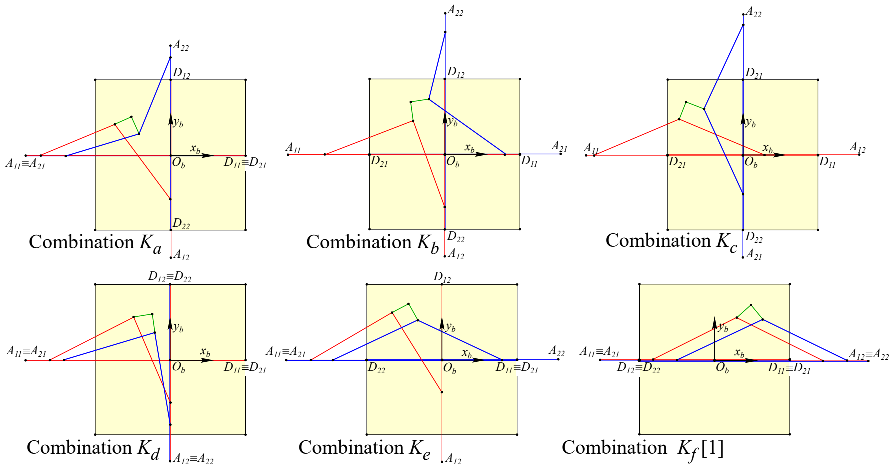

Fig. 3: Sub-workspaces combined forming the resultant workspaces.

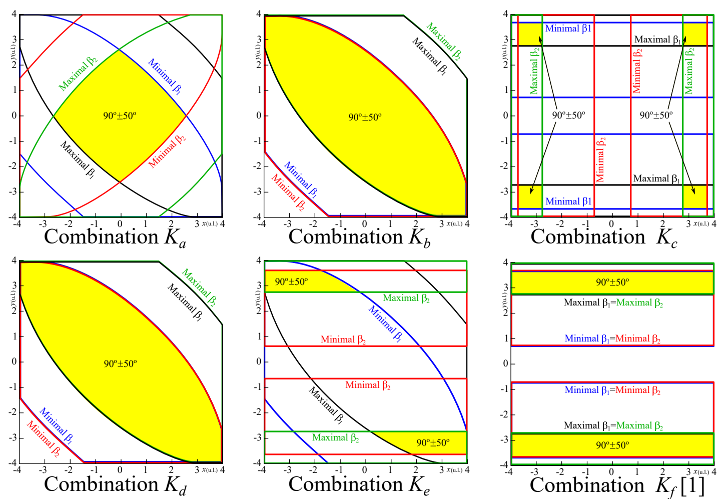

Fig. 4: Workspace regions (yellow) with transmission angles in the $90° \pm 50°$ interval.

Results shown in Fig 4 regarding the transmission angle revealed that two specific geometric configurations, K_b and K_d, exhibit the largest effective areas within the square workspace, improving the performance provided by the initial structure (K_f). This advancement over the original 4-PRR model provides a robust framework for high-performance planar motion with 360^o orientation control.

6 Conclusion

This paper advances the 4-PRR Full-Rotational Planar Parallel Mechanism (FRPPM) by extending the kinematic model formulated by Gosselin [1]. The research introduces a geometric optimization methodology prioritized by transmission quality criteria rather than purely algebraic constraints. By integrating the platform's passive angle into a Variable-Configuration (VCPMSA) framework, the proposed approach increases geometric adaptability while maintaining inherent load transfer properties.

This procedure, applicable to other full-rotation mechanisms in the literature, enhances operational performance in diverse applications requiring 360-degree orientation control.

Acknowledgements This work was supported by CNPq - Conselho Nacional de Desenvolvimento Científico e Tecnológico (National Council for Scientific and Technological Development)-Project 305344/2024-2 Brazil.

References

1. Gosselin, C., Lalibert´e, T., Veillette, A.: Singularity-free kinematically redundant planar parallel mechanisms with unlimited rotational capability. IEEE Transactions on Robotics 31(4), 969–979 (2015)
2. Ebrahimi, I., Carretero, J.A., Boudreau, R.: 3-PRRR redundant planar parallel manipulator: Inverse displacement, workspace and singularity analyses. Mechanism and Machine Theory 42(8), 1007–1016 (2007)
3. Cha, S.-H., Lasky, T.A., V´elinski, S.A.: Kinematically-redundant variations of the 3-RRR mechanism and local optimization-based singularity avoidance. Mechanics Based Design of Structures and Machines 35(1), 15–38 (2007)
4. Simoni, R., Simas, H., Martins, D.: Triflex: Variable-configuration parallel manipulators with self-aligning. Journal of the Brazilian Society of Mechanical Sciences and Engineering 37(4), 1129–1138 (2015)
5. Simas, H., Simoni, R., Martins, D.: Triflex II: Design and analysis of a self-aligning parallel mechanism with asymmetrical kinematic structure. Meccanica 52(12), 2991–3002 (2017)
6. Barreto, R.L.P., Martins, D., Simoni, R., Dai, J.S., et al.: Self-aligning analysis of the metamorphic palm of the KCL/TJU metamorphic hand. In: Proceedings of the 2018 International Conference on Reconfigurable Mechanisms and Robots (ReMAR), pp. 1–8. IEEE, Delft, Netherlands (2018)
7. Simas, H., Di Gregorio, R., Simoni, R.: Tetraflex: Design and kinematic analysis of novel self-aligning family of 3T/R parallel manipulators. Journal of Field Robotics 39(5), 617–630 (2022)
8. Meng, Q., Kesckeméthy, A., Liu, X.-J.: Motion-force interaction performance of parallel robotic mechanisms. SmartBot 1(1), 12006 (2025) [9] Rosyid, A., Al-Khasawneh, B., Alazzam, A.: Performance measures of parallel kinematics manipulators. Mechanical Sciences 11(1), 49–73 (2020)
9. Jawale, H.P., Choudhari, R.G., Thorat, H.T.: Study on transmission angle and singularity in 5R planar mechanism. Journal of Mechanical Engineering Science 238(5), 1340–1354 (2024)

10. Simas, H., Di Gregorio, R.: Local conditioning index for planar parallel manipulators. Journal of Mechanical Science and Technology 31(4), 1861–1867 (2017)